Available online at www.sciencedirect.com
ScienceDirect
Nuclear Instruments and Methods in Physics Research A 570 (2007) 22–35
NUCLEAR INSTRUMENTS & METHODS IN PHYSICS RESEARCH Section A
www.elsevier.com/locate/nima

Extensive air showers and diffused Cherenkov light detection: The ULTRA experiment

G. Agnetta[a], P. Assis[b], B. Biondo[a,c], P. Brogueira[b], A. Cappa[d,e], O. Catalano[a,c], J. Chauvin[f], G. D'Alí Staiti[a,c,g], M. Dattoli[d,e,h], M.C. Espirito-Santo[b], L. Fava[d,e], P. Galeotti[d,e], S. Giarrusso[a,c], G. Gugliotta[a,c,✠], G. La Rosa[a,c], D. Lebrun[f], M.C. Maccarone[a,c], A. Mangano[a,c], L. Melo[b], S. Moreggia[f], M. Pimenta[b], F. Russo[a], O. Saavedra[d,e], A. Segreto[a,c], J.C. Silva[b], P. Stassi[f], B. Tomè[b], P. Vallania[e,h,*], C. Vigorito[d,e], The ULTRA Collaboration

[a]*Istituto di Astrofisica Spaziale e Fisica Cosmica di Palermo, Istituto Nazionale di Astrofisica, Via Ugo La Malfa 153 - 90146 Palermo, Italy*
[b]*Laboratório de Instrumentação e Física Experimental de Partículas, Av. Elias Garcia 14, 1°, 1000-149 Lisboa, Portugal*
[c]*Istituto Nazionale di Fisica Nucleare, Sezione di Catania, Viale A. Doria 6-95125 Catania, Italy*
[d]*Dipartimento di Fisica, Generale dell'Università di Torino, via P.Giuria 1-10125 Torino, Italy*
[e]*Istituto Nazionale di Fisica Nucleare, Sezione di Torino, via P.Giuria 1-10125 Torino, Italy*
[f]*Laboratoire de Physique Subatomique et de Cosmologie, 53, avenue des Martyrs-38026 Grenoble Cedex, France*
[g]*Dipartimento di Fisica e Tecnologie Relative, Università degli Studi di Palermo, Viale delle Scienze, Edificio 18-90128 Palermo, Italy*
[h]*Istituto di Fisica dello Spazio Interplanetario dell'Istituto Nazionale di Astrofisica, corso Fiume 4-10133 Torino, Italy*

Received 30 August 2006; received in revised form 21 September 2006; accepted 23 September 2006
Available online 25 October 2006

Abstract

The Uv Light Transmission and Reflection in the Atmosphere (ULTRA) experiment has been designed to provide quantitative measurements of the backscattered Cherenkov signal associated to the Extensive Air Showers (EAS) at the impact point on the Earth surface. The knowledge of such information will test the possibility to detect the diffused Cherenkov light spot from space within the Ultra high-energy cosmic ray observation. The Cherenkov signal is necessary to give an absolute reference for the track, allowing the measurement of the shower maximum and easing the separation between neutrino and hadronic showers.

In this paper we discuss the experimental set-up with detailed information on the detection method; the in situ and laboratory calibrations; the simulation of the expected detector response and finally the preliminary results on the detector performance.

PACS: 96.40.Pq; 98.70.Sa; 95.55.Vj; 29.40.Ka

Keywords: Cosmic rays; Extensive air showers; Cosmic ray detectors; Cherenkov radiation

1. Introduction

The Uv Light Transmission and Reflection in the Atmosphere (ULTRA) experiment [1] has been designed in the context of the Extreme Universe Space Observatory (EUSO) project as a propaedeutic experimental supporting activity to study the possibility of detecting from Space the Cherenkov signal associated to the highest-energy tail of the cosmic ray spectrum. The aim of the EUSO project [2–4] is to detect the Ultra High-Energy Cosmic Rays (UHECR) by measuring the fluorescent light produced by the interaction with the Earth atmosphere. With this method, the particle track can be measured together with its relative depth, but not its absolute position. During its development through the atmosphere, the $e^{\pm}$ belonging to the Extensive Air Shower (EAS) produce a huge amount of

*Corresponding author. Istituto di Fisica dello Spazio Interplanetario dell'Istituto Nazionale di Astrofisica, corso Fiume 4-10133 Torino, Italy. Tel.: +390116707349; fax: +390116707493.
E-mail address: Piero.Vallania@to.infn.it (P. Vallania).
✠Deceased.

0168-9002/$ - see front matter © 2006 Published by Elsevier B.V.
doi:10.1016/j.nima.2006.09.102

Cherenkov photons emitted in a narrow cone along the shower axis. At the impact with the Earth surface, this light is partially absorbed and partially diffused, giving the possibility, if detected together with the main fluorescent signal, of having an absolute reference for the track, thus allowing the measurement of the shower maximum. Aim of the ULTRA experiment is to provide quantitative measurements of the reflectively diffused signal produced by the EAS impact on the Earth surface, overcoming the lack of information in this specific field.

The detection of EAS through the Cherenkov light reflected by snow was indeed firstly proposed by Chudakov [5] in 1972 and performed at the Big Alma-Ata Lake [6] (Kazakhstan) and other sites [7,8] since 1983, but only snowed surfaces were used without any measurement of the related EAS. For our purposes, since the Earth surface is covered by more than 70% of water, we need to study the diffusing properties of this medium. The study of the feasibility of the fluorescent light detection and the atmospheric background measurement by balloon borne experiments have been done elsewhere [9]; the goal of the ULTRA experiment described in this paper is to verify the possibility of detecting the reflected/diffused Cherenkov light produced by the EAS impacting on sea water. A scintillator array and an UV light detector will operate in coincidence to detect the electromagnetic component of EASs and the associated UV photons. In order to fully characterize the impinging signal, both direct and diffused light are measured. We have decided to perform these measurements in real conditions, using the same signal (i.e. lateral distribution, energy spectrum and time spread of incoming photons) that will be visible from Space, not only to have the exact features, that in any case could be reproduced in laboratory, but mainly to study the effect of the accompanying particle shower on the impacting surface. For this reason we have prepared a laboratory facility to test the properties of the incident light of fixed wavelength on different surfaces.

2. Detector layout

The ULTRA apparatus is a hybrid system composed by three main parts named ETscope, UVscope and Belenos, respectively. ETscope is a small array of scintillators which measures the shower size and the arrival direction of incoming EAS; near the centre of the array are located two couples of wide field Cherenkov light detectors, called "Belenos",[1] pointing to zenith and nadir to measure in coincidence the direct and diffused Cherenkov light.

Outside the array is sited UVscope, made by a couple of narrow field Cherenkov detectors pointing to the centre of the array; it is used to give the most accurate measurement of the diffusion coefficient. The first tests were performed during October 2002 and June–July 2003 at Mont-Cenis (France, 1970 m a.s.l.) and during 2004 at LPSC, Grenoble (France, 250 m a.s.l.) to test, calibrate and optimize the detectors [10]; in May 2005 the experiment was carried out at sea level in a small private harbour in Capo Granitola (Italy) [11]. In this paper we describe the characteristics and performances of the final experimental set-up.

2.1. ETscope: the electromagnetic detector

The electromagnetic detector ETscope is a small EAS array made by five particle detection stations. Each station includes a plastic NE102A scintillator ($80 \times 80\,cm^2$ area and 4 cm thick) with an expected light yield of ~40 photoelectrons/m.i.p. (minimum ionizing particle). Two photomultipliers XP3462, with high voltage power supplies set to work at different gains (High Gain (HG) and Low Gain (LG) photomultipliers) are located below each scintillator at a distance of 30 cm. Both the scintillators and the photomultipliers are contained in a pyramid-shaped box made of stainless steel and coated with white diffusing paint. All the equipment is finally housed in a $1\,m^3$ plastic container to provide total insulation. The main goal of this detector is to determine the arrival direction, size and core location of the impinging shower. This information, together with the UV-light measurements and an accurate Monte Carlo simulation, will determine the diffusion features of the selected surface.

Designed to be operated on different environments including the sea, the ETscope has been optimized as a portable, floating and waterproof detector. At the Capo Granitola site four out of five stations were placed at the vertexes of a trapezoid at different heights on the shore surrounding the bay as illustrated in Figs. 1 and 2. Being the bay very well protected from waves, tides and winds, we managed to place the fifth scintillation counter on a raft in the middle of the experimental area.

2.2. UVscope: the narrow field of view optical device

The UVscope optical device, as shown in Fig. 3, consists of two separate units (telescopes) placed on a tripod. The telescopes are mechanically aligned to have parallel optical axes; each telescope is made of a common Fresnel lens of 0.46 m diameter having a large Photo-Multiplier Tube (PMT) on its focal plane. The lens provided by Fresnel Tecnologies Inc. [12] is made of UV transmitting acrylic material which offers a good optical quality with bulk transmittance approaching 90% in the wavelength band of

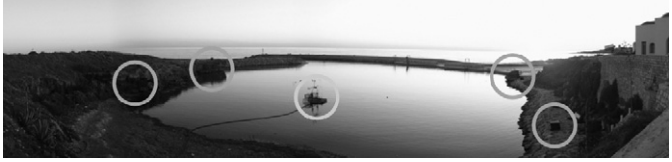

Fig. 1. The ULTRA experiment at Capo Granitola, Italy.

[1]Belenos was the Celtic god of light, a Gallo-Roman nickname for Apollo, often invoked by Asterix and the other Gauls.

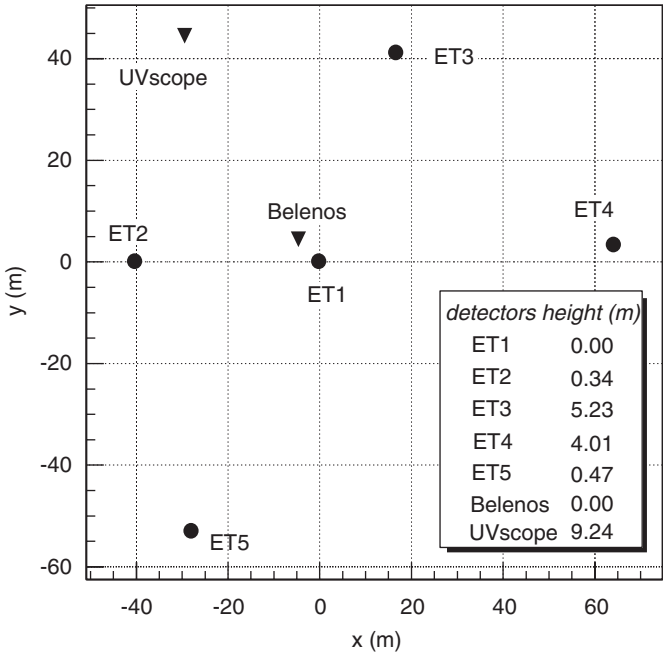

Fig. 2. Position of the detectors in the local reference system.

Fig. 3. UVscope in the Lab.

interest (300–600 nm). The PMT used is the EMI D319QB, which features a large diameter (91 mm) bi-alkali photocathode, a fused silica window, and a Quantum Efficiency (QE) of ~22%@420 nm. The PMT is housed in a cylindrical aluminium container together with the voltage divider circuit; the diameter of the exposed side of the photocathode is reduced to 72 mm by means of a Teflon flange. At the top of the container a slot allows the insertion of a filter. The lens and the PMT envelope are housed in a bigger cylindrical aluminium container with the PMT window centred on the axis of the cylinder and at a distance of 46 cm from the lens. The cross-section of the assembled telescope that includes a light baffle is shown in Fig. 4.

2.3. Belenos: the wide field of view optical device

The direct incoming Cherenkov light (i.e. before any reflection) is monitored by a small telescope (named Belenos) located near the centre of the array and pointing to Zenith. The Belenos is a wide field of view binocular system, each ocular being composed by two Fresnel lenses, focusing the incoming light onto a $\frac{1}{2}$ in. diameter PMT. The lenses are made in borosilicate, which allows transmissions down to 300 nm. The first lens has a diameter of 20 cm, and its overall thickness of 6 mm allows refraction of incident light up to $\theta = 40^{\circ}$, collecting it on an area of 10 cm diameter at the focal distance of 10 cm. The second lens, with a diameter of 8 cm, is located on the focal plane of the first one. This second lens focuses the collected light on its focal plane at 4 cm where a BG3 filter and the photomultiplier photocathode are located (see Fig. 5).

3. ULTRA data acquisition

The ULTRA DAQ is based on custom-made PCI data acquisition boards, LIP-PADs [13], installed on a PC. The LIP-PAD is a multi-purpose PCI data acquisition board that digitizes analogue signals with a frequency of 100 MHz and a 10 bit precision in the range 0–1 V. It is also capable of measuring time differences with a precision of few ns and a dynamic range greater than 1 s. The main blocks of LIP-PAD (Fig. 6) are the Time Measuring Subsystem (TMS) and the Analogue Acquisition Subsystem (AAS). The TMS comprises a TDC and digital clocks with a frequency of 50 MHz. The AAS is made by six analogue

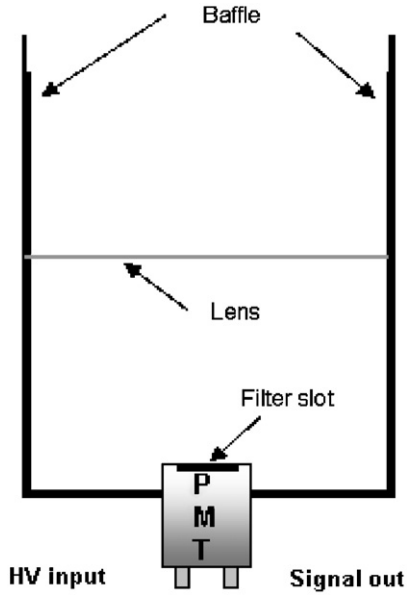

Fig. 4. Cross-section of each UVscope telescope.

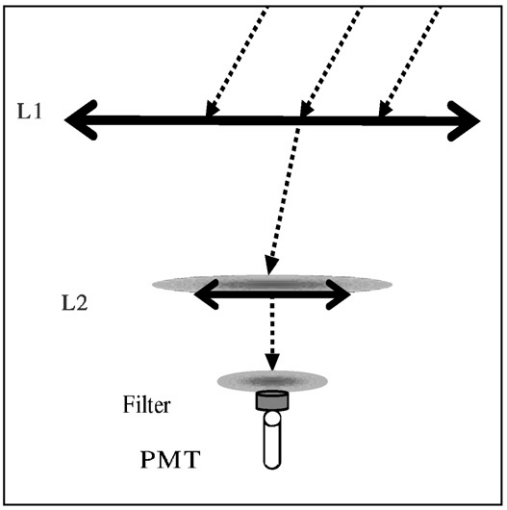

Fig. 5. Schematic drawing of the Belenos eye.

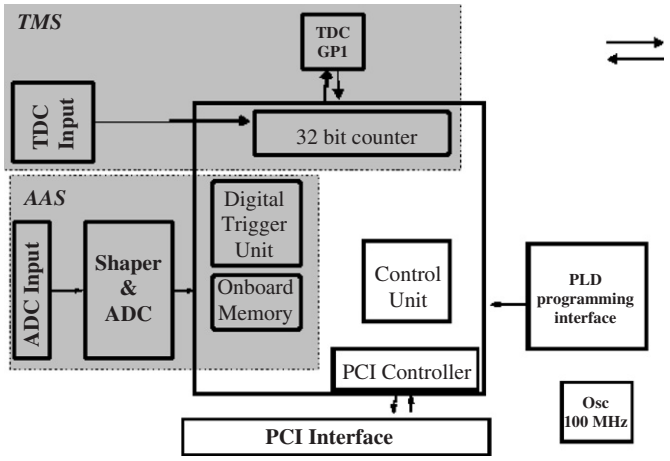

Fig. 6. Block diagram of the LIP-PAD Board.

acquisition channels, each having a shaper, an amplifier and a 10 bit FLASH ADC. The analogue signals are shaped and amplified and digitized by the ADC and then written to a buffer memory. The digital trigger unit can implement various trigger conditions (e.g. simple threshold, muon, double pulse, shower). The board is read by and controlled through the PCI protocol. The core of the board is a programmable logic device in which the control logic (PCI protocol, status and signal control), the logic associated with the TMS and the logic related with the analogue acquisition are implemented.

Four LIP-PAD boards are used by the ULTRA DAQ to acquire the output signals of the PMTs of the several detectors (Fig. 7). In order to assure the required accuracy on the determination of the arrival direction, and to correctly join the information collected by different boards, two synchronization requirements must be satisfied:

- time differences between the ETScope HG PMT signals must be measured with a precision of 10 ns. On the same board this is obtained as the 100 MHz ADC clocks of all ADC are common;
- signals must be identified as belonging to the same event. The synchronization between different LIP-PADs is achieved by the common trigger signal to the level of few tens of ns.

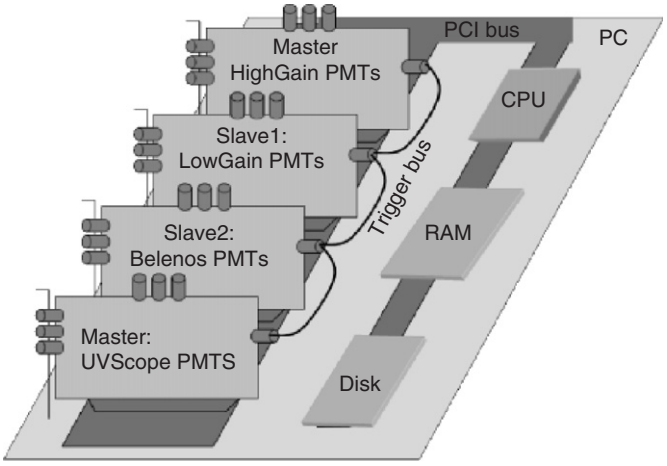

Fig. 7. Scheme of the DAQ system using four LIP-PADs.

3.1. Software

The DAQ software is based on LabView. The core of the Acquisition software is a basic routine that allows reading and writing on any memory address of the PCI bus. The software controls the flow of information and implements an user-friendly Graphical User Interface (GUI) that allows the user to configure the trigger parameters, to select the number of events to be acquired and the file in which the acquired data are to be written. Data are saved as a binary file containing an event header of 256 bytes followed by 24×256 bytes that correspond to the ADC values registered on all channels of the four boards in an event.

3.2. System performance and data processing

This DAQ system based on LIP-PADs was tested in comparison with a traditional one based on CAMAC and NIM. The system proved to be efficient and reliable, reproducing the results from the CAMAC system with the benefit of lesser saturation. The experiment gained also a sampling of the signals in time which was not possible with the CAMAC system. This feature is essential to discriminate particle and diffused Cherenkov light signals in the UVScope. Also, the signal integration window is made as small as the signal width, reducing the noise integrated. The noise present in the signal can be estimated using the pre-trigger data recorded before the measurement; the trigger threshold is set according to this background level. The trigger is flexible and does not require an extreme precision as a time window of 2.5 μs of data is recorded

around the trigger. During the Capo Granitola experiment a four-fold coincidence on the HG PMTs of the on-shore stations was the required condition to trigger the data acquisition on all available detectors.

The information on charge and timing are extracted from the digitalized signal under ROOT platform (see sample in Fig. 8). A digital trigger is implemented to identify possible signals: the first point exceeding 5σ fluctuation above the baseline recorded in the pre-trigger data (400 ns range) is searched. To extract interesting features of the shape, an empirical parameterization of the signal, which describes the fast charge and the lower discharge of a capacitor, is used

$$V(t) = C \cdot e^{-1/2w^2 \cdot \log^2((t-x_0)/\Delta)}. \quad (1)$$

C is the value at maximum, w is the length of the signal, x_0 is the start time and Δ is the rising time. When a signal is identified, the shape is fitted to function (1) and the charge Q (amplitude integration along the optimal fitted shape) and the start time t_{20} (constant fraction time at 20% of the maximum amplitude) of the pulse are extracted. Event by event all data regarding the five ETscope stations are analysed following the discussed procedure for both HG and LG photomultipliers, with the prescription that t_{20} is always obtained from HG PMTs, while for charge measurement LG PMT is used when the corresponding HG PMT is saturated.

For the Belenos and the UVscope units, since the expected signal is weaker, the fit method is not suitable to process registered pulses and a simpler approach is applied. First, background level is estimated on the pre-trigger data.

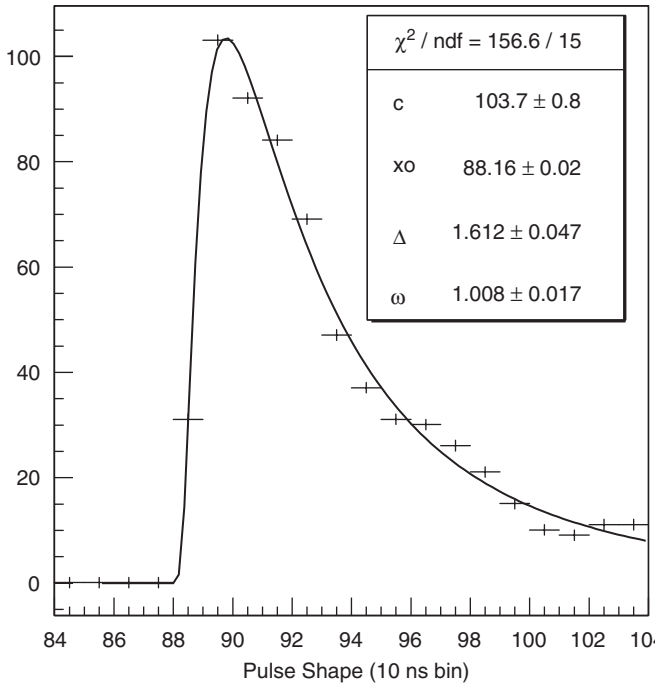

Fig. 8. The digitalized pulse shape of one ETscope station contained in the 2.5 μs and the reconstructed fit: values of free parameters are shown. Baseline has been subtracted.

The start time x_0 of the pulse, if any, is the first point exceeding 5σ fluctuation above the baseline while the charge Q corresponds to the amplitude (background subtracted) integration over a window with variable width, from x_0 till the signal decay under the baseline level. This method improves the S/N ratio compared to a fixed gate integration.

4. Shower parameters reconstruction

The charge values obtained with the procedure discussed in the previous section must be converted to Vertical Equivalent Muons (VEM) before being used to reconstruct the shower lateral distribution and size. The calibration procedure for both HG and LG PMTs is the following: first the high voltage for both PMTs has been selected to see the full spectrum with background component, valley and muon peak avoiding any effect due to the trigger threshold. Then HG photomultiplier calibration was achieved through the direct measurements of single muon spectrum by triggering the DAQ by the coincidence of the two PMTs. The VEM charge, corresponding to the average value of the measured spectrum corrected by the mean crossing angle 36.9° [14], is then the calibration factor used to convert the measured charge in the equivalent particle density on each detector. At this point the LG PMT voltage was reduced by 300 V. Its calibration was performed by cross-correlation with the corresponding HG PMT on a set of selected events, requiring: (a) no saturation effect on the full pulse shape and (b) time difference $\delta t < 30$ ns between reconstructed starting times of the HG and LG PMTs pulses. The ratio between high and LG PMTs is $R \simeq 10$: the observed ADC saturation is ~50 and 500 VEM/m^2 for HG and LG, respectively. If ADC saturation is present on the HG PMT shape, LG data are used to measure the particle density.

4.1. Arrival direction reconstruction and resolution

EAS arrival direction is obtained event by event using the times of flight between different modules. The shower structure, i.e. the disk curvature and thickness, affects the measurement of the arrival direction. However in our case, due to the small dimensions of the ETscope array compared to the lateral spread of the shower, a plane shower front can be assumed. The time zero t_0 correction (i.e. the absolute time differences with respect to the central station used as reference), which accounts for different cables length, transit time in the photomultipliers and electronic delays, was experimentally measured during calibration runs with the detectors superposed two by two, and included in the arrival direction reconstruction. The θ and ϕ distributions are shown in Fig. 9.

The angular resolution is undirectly estimated through a check of intrinsic consistency of data. Events firing all five stations and fully reconstructed have been considered. The resolution is obtained from the measurement of

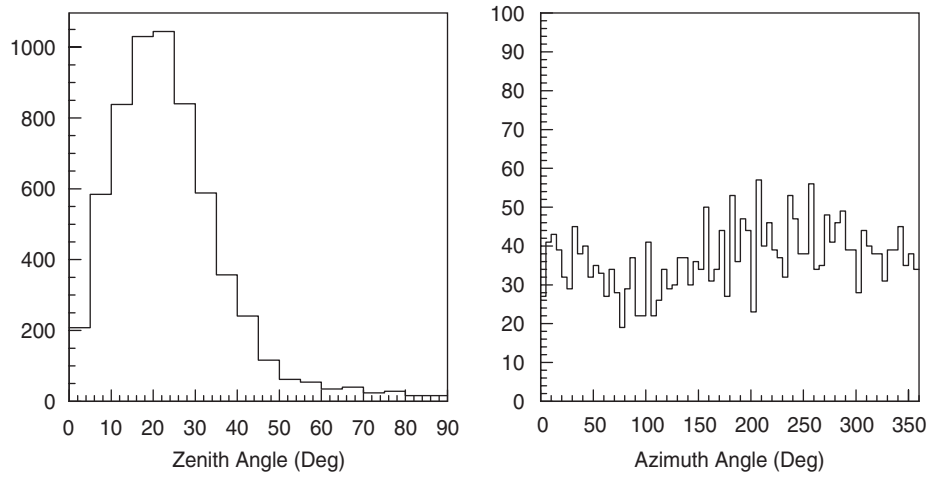

Fig. 9. Arrival direction: θ and ϕ (for $\theta<20^\circ$) distributions.

time-of-flight fluctuation which includes counter and PMT performances and systematic effects due to the pulse shape processing. We assume that all detectors are equivalent for what concerns electronic chain and way of processing the pulse shape: results obtained on a detector can be extended to all ETscope stations. The ETscope configuration (see Fig. 2) shows that in a rough approximation the line connecting counters ET2 with ET3 and that connecting ET4 with ET5 are almost parallel and lie in a plane. Therefore, the time-of-flight differences $\Delta T_{2,3}$ and $\Delta T_{4,5}$ are affected only by the geometrical separation $L_{2,3} = 70.5\,\mathrm{m}$ and $L_{4,5} = 108.1\,\mathrm{m}$ and do not depend from the shower arrival direction. From this hypothesis the measured value $\Delta T_{2,3}$ can be compared with the expected one $\Delta T'_{2,3}$ obtained by the normalization of the total time-of-flight $\Delta T_{2,3} + \Delta T_{4,5}$ to the proper travelled distance $L_{2,3}$:

$$\Delta T'_{2,3} = \frac{L_{2,3}}{L_{2,3} + L_{4,5}} \cdot (\Delta T_{2,3} + \Delta T_{4,5}). \quad (2)$$

The spread of $\Delta = \Delta T'_{2,3} - \Delta T_{2,3}$ is connected to the spread of each component $\Delta T_{i,j}$, i.e. the time resolution in the time difference measurement. That is

$$\Delta = k \cdot (\Delta T_{2,3} + \Delta T_{4,5}) - \Delta T_{2,3}, \quad k = \frac{L_{2,3}}{L_{2,3} + L_{4,5}},$$

$$\sigma^2_\Delta = 2 \cdot (k \cdot \sigma_{\Delta T})^2 + \sigma^2_{\Delta T}.$$

The resolution on the time-of-flight $\sigma_{\Delta T} = \sigma_\Delta / \sqrt{2 \cdot k^2 + 1}$ is obtained in fixed bins of zenith angle.

Finally the data set has been reprocessed. Event by event a random time contribution, fluctuated over a Gaussian $(0, \sigma_{\Delta T})$ distribution, is added to each $\Delta T_{i,j}$ used to triangulate the shower arrival direction. The fluctuated zenith angle Θ_f is calculated with new values $\Delta T'_{i,j}$. The resolution corresponding to the spread of the distribution of the $(\Theta - \Theta_\mathrm{f})$ values is shown in Fig. 10 as a function of the zenith angle.

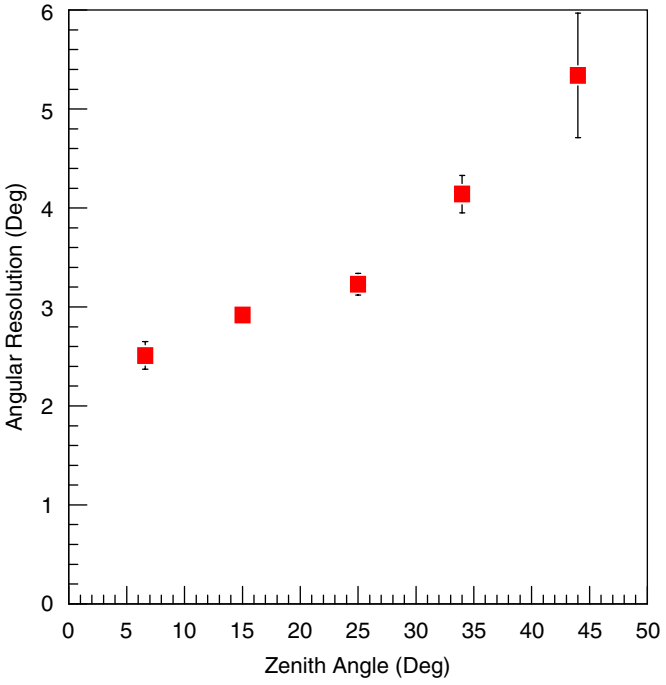

Fig. 10. Zenith resolution on arrival direction as a function of the arrival direction up to 50°. At larger zenith angle statistics is very poor: resulting resolution is affected by a big systematic error.

4.2. Core position and shower size determination

After the VEM measurement on each counter, events are divided into two main subsets: internal and external. The internal subset includes only the events in which the recorded number of particles in the central floating station is greater than the number registered in the external ones: being ET1 the central detector, this means $n_{\mathrm{ET1}} > n_{\mathrm{ET}i}$ for $i = 2, 5$ (see Fig. 2).

Shower size and core position are calculated from the measurement of particles densities in the five ETscope stations for all the events of which the arrival direction has been reconstructed. Event by event, counter positions are

projected into the plane perpendicular to the arrival direction and containing the central detector. The reconstruction is performed by means of a χ^2 fit in which particle densities recorded by each module are compared with the theoretical NKG lateral distribution:

$$\rho(r) = k(N_e/r_0^2)(r/r_0)^{s-2}(1 + r/r_0)^{s-4.5}. \quad (3)$$

Due to the low number of samplings, fixed values of the shower age parameter $s = 1.2$ and of the Molière radius $r_0 = 100$ m are assumed.

The fitting procedure is the following:

- counters positions are projected into the plane perpendicular to the arrival direction;
- preliminary core position, assumed to be the baricentre, is the starting point for the fit minimization; initial size is fixed to $N_e = 10^5$;
- MINUIT migration is performed: core positions on the x and y-axes are bounded within 100 m around the central station and size reconstruction is limited in the 10^3-10^7 range. Minimization is achieved if $\chi_0^2 < 15$;
- shower size and core position, back projected into the array plane, are saved for further analysis.

All minimizations are performed using the CERN library MINUIT under ROOT platform. Figs. 11 and 12 show the distribution of core positions and size spectrum for internal events. As expected, the core of these events is located around the central station and confined in a region fixed by the shape of the lateral distribution function. They are ~25% of the full set of data and correspond to the best reconstructed sample.

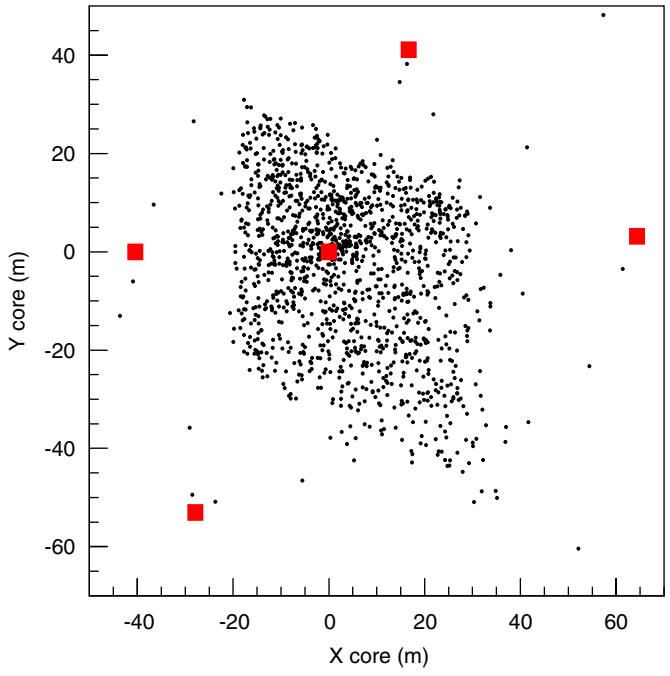

Fig. 11. Core position in the detector plane: obtained values correspond to the expected geometrical distribution for internal events.

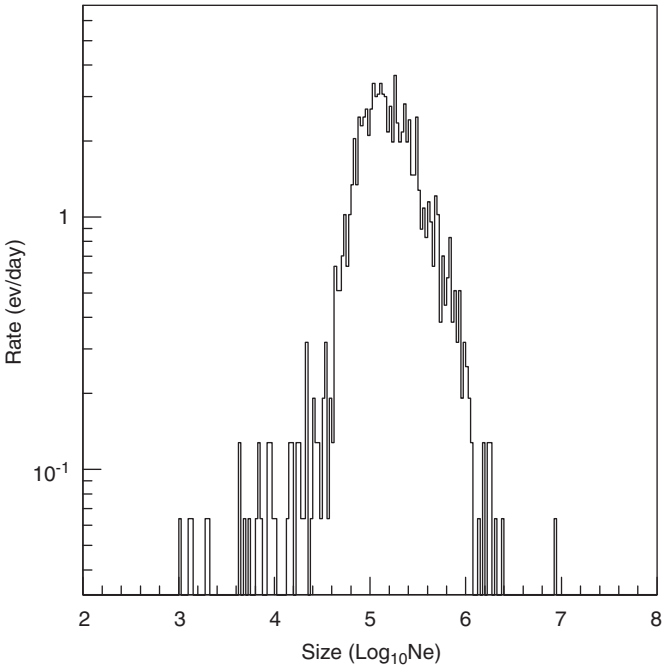

Fig. 12. The shower size distribution for internal events.

4.3. Effective area and shower size resolution

EAS were developed with the Monte Carlo code COsmic Ray SImulation for KAscade (CORSIKA6.015) [15] from primary protons using QGSJET hadronic interaction model for high-energy interactions and GHEISHA2002 for low-energy interactions. About 2000 showers were simulated for seven selected energy values, ranging from 10^{14} to 10^{16} eV, and two zenith angles, $\theta = 0^\circ$ and 20°. The simulations were repeated at two observation levels, 0 and 2000 m a.s.l., in agreement with tests and experimental runs. NKG option was used to reduce the computing time. The used sampling area for shower cores increased with energy and ranged between 2.9×10^3 m^2 at 10^{14} eV and 4.7×10^4 m^2 at 10^{16} eV.

The CORSIKA output was used to estimate the ETscope performance for showers of different energy and inclination, using a specific detector simulation program. The response of each ETscope module was simulated taking into account the Poissonian and experimental fluctuations of the number of particles. The experimental trigger conditions were applied: the four-fold coincidence between the external stations is the basic requirement to select the events. Moreover, since the UVscope field of view is very narrow, covering a small area around the array centre, only internal events are selected. Finally, the reconstruction of core location and shower size is given by a NKG lateral distribution function fit of the particle density on each station with three free parameters and fixed age and Molière radius (as for the experimental events). This simulation was used to optimize the energy threshold and to determine the shower size and core position resolution.

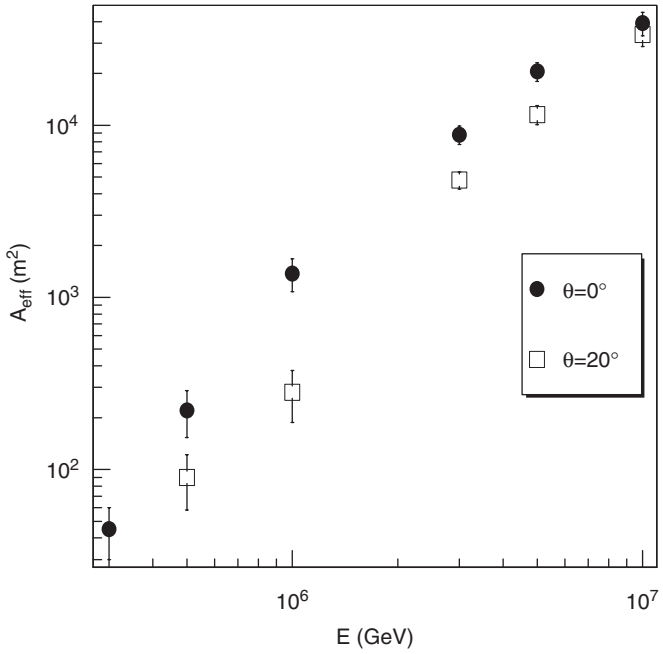

Fig. 13. Effective area of ETscope ground array.

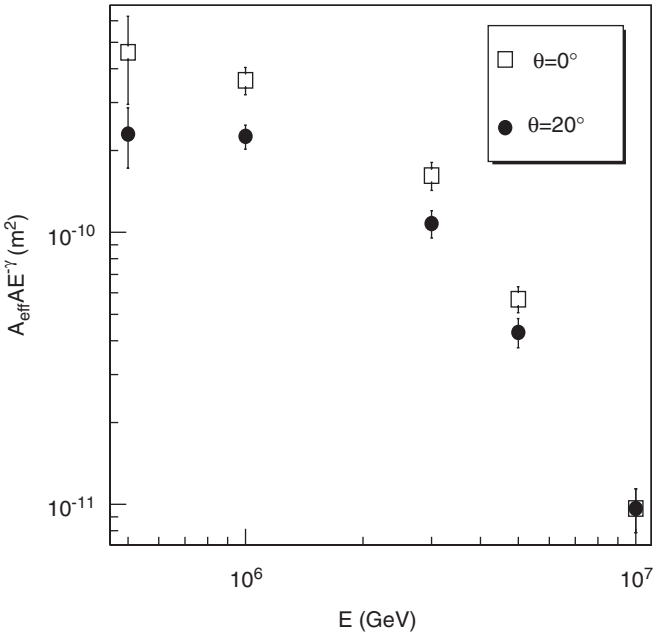

Fig. 14. Convolution between effective area and differential spectrum of the cosmic radiation.

Fig. 13 shows the effective area at sea level for protons with 0° and 20° zenith angles. The convolution between the effective area and the differential cosmic ray spectrum gives the estimation of the ETscope threshold energy. For sake of simplicity, we used an all particle spectrum made by primary protons only:

$$\phi(E)\,\mathrm{d}E = AE^{-\gamma}\,\mathrm{d}E$$

where $A = 2.8 \times 10^4$, $\gamma = 2.7$ for $E < 3 \times 10^{15}$ eV and $A = 1.1 \times 10^7$, $\gamma = 3.1$ for $E > 3 \times 10^{15}$ eV [16]. Fig. 14 shows our result: defining the EAS array energy threshold as the mode of this distribution, we obtain $E_{\mathrm{th}} \sim 10^{15}$ eV. To maximize the number of useful events, i.e. events with both components detected, the electromagnetic threshold must match the Cherenkov light detection threshold.

The goodness of the simulation was checked by comparing the expected counting rate versus the experimental one. We used the same all particle spectrum with only primary protons, as in the threshold energy calculation; the comparison with the two simulated zenith angles was done by integrating the experimental counting rate in a 10° cone around the zenith for vertical showers and between 10° and 30° for $\theta = 20°$. The results are listed in Table 1; the good agreement between experimental data and simulation proved the reliability of the simulation chain.

The shower size and core location resolutions were estimated with a Monte Carlo, by comparing the actual quantities with the reconstructed ones. Since the comparison was made for internal events only, the used sampling area ranged from $100 \times 100\,\mathrm{m}^2@10^{14}$ eV to $200 \times 200\,\mathrm{m}^2@10^{16}$ eV, comparable to the array surface. The reciprocity method [17] was used to minimize the computing time. The values obtained for events with $\theta = 20°$ are shown in Figs. 15 and 16: for $E = 10^{15}$ eV, $\Delta N_e/N_e \sim 35\%$ and $\Delta r \sim 5$ m.

Table 1
Expected and experimental counting rates of Capo Granitola events

$f^{\mathrm{tot}}_{\mathrm{MC}}(\theta < 30°)$	$f^{\mathrm{tot}}_{\mathrm{exp}}(\theta < 30°)$
$(3.32 \pm 0.19) \times 10^{-3}$ Hz	$(3.49 \pm 0.12) \times 10^{-3}$ Hz
$f^{\mathrm{int}}_{\mathrm{MC}}(\theta < 30°)$	$f^{\mathrm{int}}_{\mathrm{exp}}(\theta < 30°)$
$(6.38 \pm 0.31) \times 10^{-4}$ Hz	$(6.69 \pm 0.54) \times 10^{-4}$ Hz

5. Calibration and performance of the Cherenkov light detectors

In order to compare the charge measured by the PMTs connected to the Cherenkov light detectors with the MC expectations, an accurate calibration allowing the conversion from the digitalized shape to the number of photons on the top of the external lens is required. This includes the measurement of the single photoelectron for both UVscope and Belenos telescopes; in addition, the efficiency and transmission of the different parts of the detectors along the optical path must be considered. Moreover, since the Belenos have a wide field of view, the efficiency as a function of the incoming photons angle must be obtained. Finally, the background measurement, essentially connected to the detection energy threshold, can be used to check this charge to photons conversion.

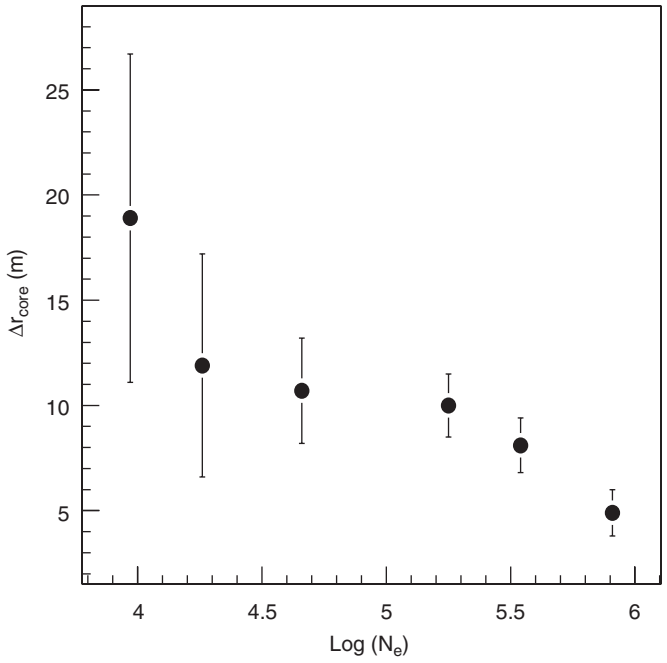

Fig. 15. Resolution in the reconstruction of core position for $\theta = 20^\circ$.

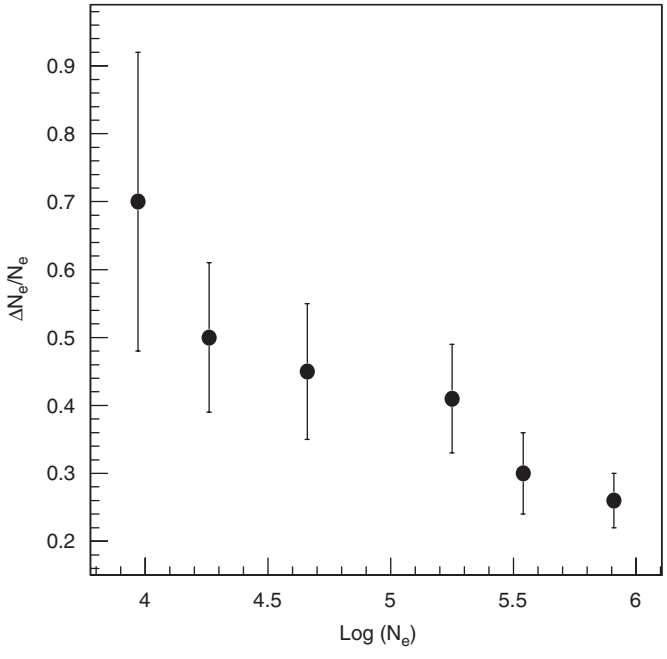

Fig. 16. Resolution in the reconstruction of size for $\theta = 20^\circ$.

5.1. UVscope calibrations

The Single Photon Counting technique was used to measure the equivalent $\langle pe \rangle$ (mean value of the measured photo-electron spectrum of integrated pulses) in units of LIP DAQ channel (mV 10 ns) at a suitable fixed operating HV. Relative calibration between the PMTs of the two UVscope telescopes was carried out using the measurement set-up shown in Fig. 17. The $\langle pe \rangle$ was 1.1 LIP DAQ units for PMT1 and 1.48 for PMT2.

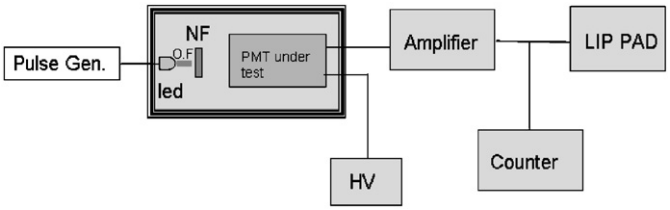

Fig. 17. A lightproof box, internally black painted, houses a blue led connected via a lightproof connector to a Pulse Generator and the PMT connected to external HV channel and to a signal amplifier. An optical fiber wire takes the pulsed light from the led to the PMT photo-cathode. A 10% neutral filter intercepting the led light path, allows operating in single photon counting mode.

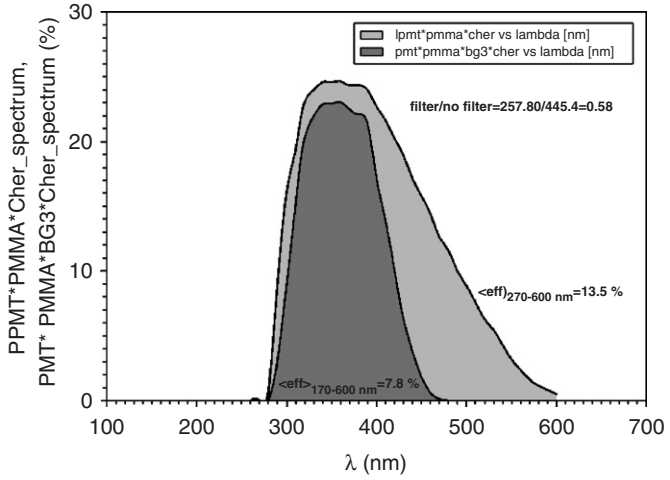

Fig. 18. The UVscope total efficiency.

Then, the average total efficiency of the UVscope telescopes has been calculated convolving the efficiencies of lens, PMT and Cherenkov spectrum with and without the BG3 filter. The values so obtained are 7.8% and 13.5%, respectively, as shown in Fig. 18. These values were used to convert signal pulses into the equivalent number of photons seen by the UVscope.

5.2. Belenos calibrations

The effective light collection surface of the Belenos as a function of the wavelength and the incident angle was studied to correctly determine the number of Cherenkov photons reaching the array.

The optics configuration with the second lens placed at the focus of the first one, was chosen in order that the collection area would be larger than the PMT area alone. The total transmission spectrum through lenses, filter and PMT QE is shown in Fig. 19 for a normalized vertical Cherenkov light spectrum ($1/\lambda^2$); in this case the overall QE is 9.4%.

Due to its peculiar geometrical configuration, Belenos optics on the whole is more efficient for large incoming angles, as shown in Fig. 20.

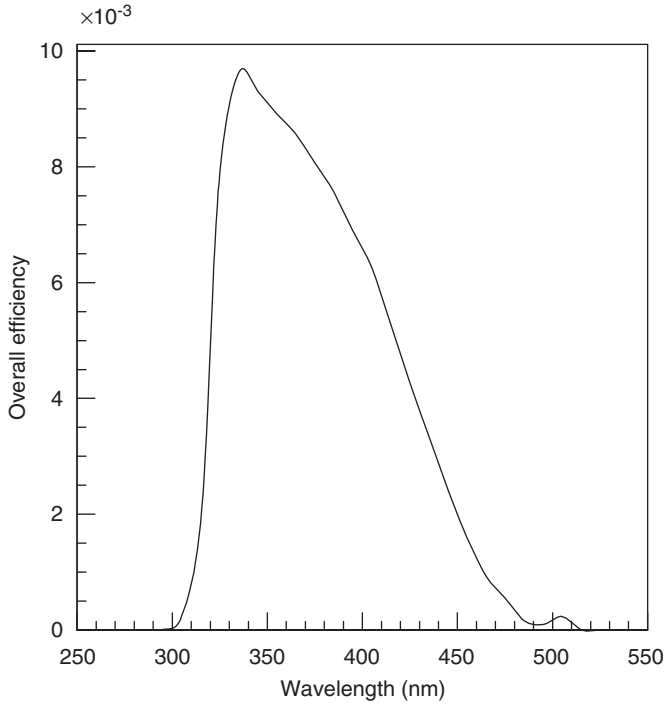

Fig. 19. Overall efficiency for Cherenkov light as function of wavelength.

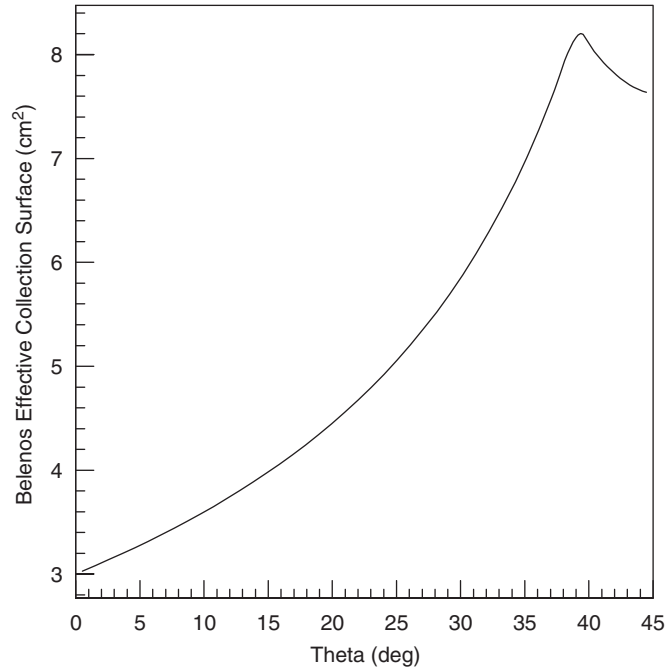

Fig. 20. Belenos effective collection surface (cm^2).

5.3. Background measurements

Measurements of diffused background light were carried out at the Capo Granitola site during a moonless night (25–26 May 2005). The detector used was the PMT Hamamatsu R3878 with known QE working in single counting mode and coupled with a BG1 filter. A collimator was used to reduce the detector field of view to 0.01 sr with a resulting Geometrical Factor of $2.45 \times 10^{-7}\,m^2\,sr$. The detector was pointing to the sea water with the same inclination and direction of the UVscope. The measurements gave an average diffused background of 680 photons/(m^2 ns sr).

The level of diffuse background can also be roughly estimated directly by using the UVscope acquisition data, and with the formula:

$$\langle B\rangle = N_{pe}/(A * \Omega * \Delta t * \varepsilon_{\mathrm{tot}}) \tag{4}$$

where, for each telescope, N_{pe} is the total number of photo-electrons, A is the lens collecting area, Ω is the solid angle, Δt is the time window, and $\varepsilon_{\mathrm{tot}}$ is the total efficiency. For each telescope, in the wavelength band 270–470 nm (filter window), the total efficiency can be defined as

$$\varepsilon_{\mathrm{tot}} = QE(\lambda) * CE_{\mathrm{pmt}} * T\varepsilon_{\mathrm{lens}}(\lambda) * T\varepsilon_{\mathrm{filter}}(\lambda) \tag{5}$$

where $QE(\lambda)$ is the PMT QE (which depends on the wavelength), CE_{pmt} is the PMT collecting efficiency, and $T\varepsilon_{\mathrm{lens}}(\lambda)$ and $T\varepsilon_{\mathrm{filter}}(\lambda)$ are the transmission efficiency of lens and filter, respectively, which depend on wavelength.

To evaluate N_{pe} we used UVscope data recorded under two different working conditions: UVscope covered (close to external light) but functionally operating, and UVscope uncovered (normal acquisitions). In both cases, we considered the signal recorded in the first 50 ADC channels, after ADC pedestal subtraction; in that range we are confident that, due to the trigger set-up, there are no signals from shower particles (remember that trigger is set to channel 128, in the middle of the acquisition window). The mean value of the signal in that region is (substantially) due to the dark current of the PMT when the UVscope is covered whereas, with the UVscope uncovered, it is the sum of diffuse background plus PMT dark current. For each telescope, if we define $\langle L_{\mathrm{c}}\rangle$ and $\langle L_{\mathrm{u}}\rangle$ the means of the light measured in LIP DAQ unit under covered and uncovered configuration, respectively, the quantity $\langle L\rangle = \langle L_{\mathrm{u}}\rangle - \langle L_{\mathrm{c}}\rangle$ represents the light intensity entering in the telescope and hence the diffuse background light. By dividing $\langle L\rangle$ by the equivalent $\langle pe\rangle$ correction factor, the total number of photo-electrons N_{pe} is obtained. With this method we obtained average values of diffuse background equal to 755 and 880 photons/(m^2 ns sr) for the two telescopes. Taking into account that the covered and uncovered data were recorded in different days and for different exposure times, the results of the diffuse background estimation can be considered in agreement with the values obtained through the PMT Hamamatsu R3878 measurements. In any case, the diffuse background level for data analysis has been always evaluated event by event on the basis of the average value of the first 50 DAQ channels.

5.4. Cherenkov light energy threshold

The lateral distribution functions of the Cherenkov photons were simulated using the same Monte Carlo code CORSIKA6.015 [15] used for ETscope. In this case, the EGS4 model of electromagnetic interactions was used to simulate the Cherenkov light production instead of the NKG option. Energy thresholds of 500 MeV for hadrons and muons and 3 MeV for electrons and γ were used. Lateral distributions of Cherenkov photons in the wavelength band [300, 450] nm at 2000 m a.s.l. and at sea level were obtained for showers generated by primary protons of fixed energy in the range $[10^4-10^7]$ GeV for two different values of the zenith angle (0° and 20°). Showers from primary protons of $E = 10^6$, 3×10^6 and 5×10^6 GeV were simulated also with zenith angles 10°, 30° and 40° for sea level observation. As shown in Fig. 21, the lateral distribution of Cherenkov light has a relatively flat region up to distances of about 120 m from the shower core. The lateral distribution functions (LDF) obtained from the simulations were fitted with a rational equation of three parameters of the form $Q = a/(b + cR)$, where R is the distance from the shower axis.

These lateral distributions were used to evaluate the signal-to-noise ratio (SNR) of Belenos using the geometrical parameters measured in the Capo Granitola campaign. The threshold energy for detecting a direct Cherenkov light signal must be carefully evaluated in order to match the electromagnetic threshold energy. With the measured background, the expected noise in a Belenos unit can be calculated with the following formula:

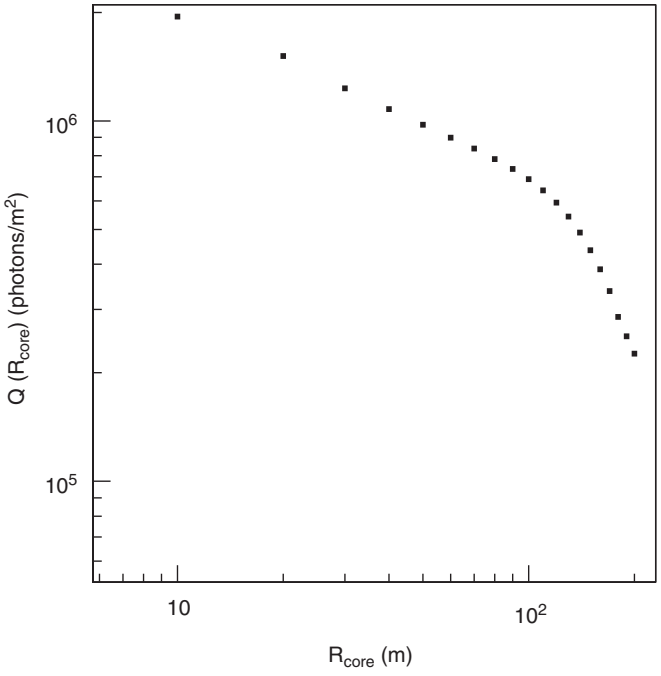

Fig. 21. Lateral distribution function of a shower ($E = 5 \times 10^6$ GeV, $\theta = 20°$).

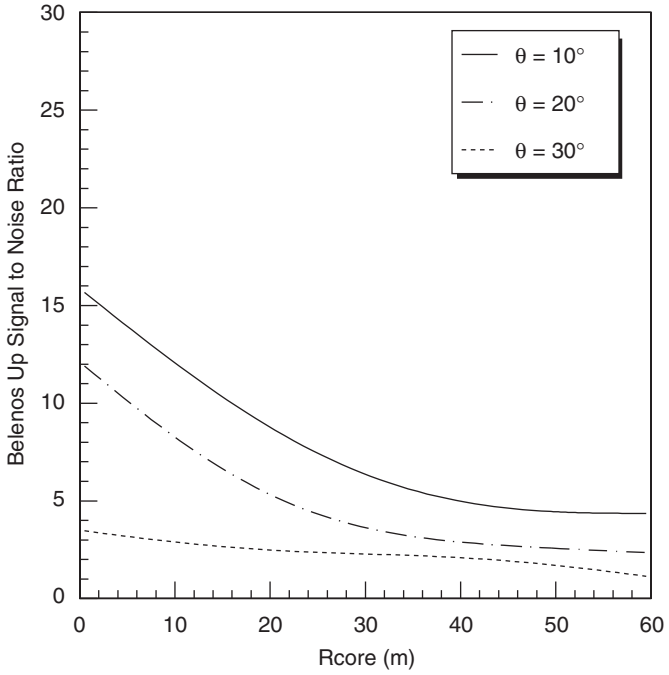

Fig. 22. Belenos up signal-to-noise ratio versus Rcore ($E = 3 \times 10^6$ GeV).

$$\text{Noise} = CS_{\text{eff}} \cdot \langle \text{bkg} \rangle \cdot \Delta t \cdot \varepsilon$$

where CS_{eff} is the integral of the collecting surface on the solid angle set by the field of view, $\langle$bkg$\rangle$ is the mean value of the background ($\sim$800 photons/(m^2 ns sr) at the observation site), Δt is the integration time (assumed to be 300 ns) and ε is the total efficiency of the detector. With these values the mean noise contribution is expected to be $\sim 1.3 \times 10^4$ photoelectrons per event.

The number of photoelectrons due to Cherenkov photons was calculated with the formula:

$$N_p e = N_{\text{Cer}} \cdot CS_{\text{eff}}(\theta) \cos(\theta) \varepsilon$$

where N_{Cer} is the number of Cherenkov photons directly hitting the area of the first lens, calculated with the simulated lateral distribution functions for the chosen arrival direction and core distance. The SNR, i.e. the intensity of the signal divided by the fluctuation of the noise, was calculated for fixed energy values as a function of the core distance for different values of the arrival direction. Fig. 22 shows that the sensitivity of the Belenos is greater than 3σ for primary energy $E = 3 \times 10^{15}$ eV, core distances $\leqslant$50 m and zenith angle $\leqslant 30°$, and it is greater than 5σ if the zenith angle is in the range $[10°, 20°]$. According to this threshold energy value, the expected counting rate for $\theta \in [15°, 25°]$ is $[2.73 \pm 0.38] \times 10^{-4}$ Hz; this value matches the experimental counting rate ($[3.26 \pm 0.20] \times 10^{-4}$ Hz) of events with a signal detected in both Belenos and arrival directions in the same angular range.

6. Laboratory measurement of ground reflectance

In order to compare the results obtained with the real Cherenkov light, i.e. photons accompanying the EAS

development in the atmosphere, with the photons alone, a dedicated reflectometer has been built. A cooled Deuterium lamp was coupled to a grating monochromator to deliver light at selected wavelength onto a bundle of quartz fibers. The fiber was guided into a dark vessel where it was mounted and fixed on one arm of a two-arm semi-spherical goniometer. The head of the fiber, equipped with a lens, illuminated a horizontal area at the goniometer centre where the sample was located. The other arm was equipped with a $\frac{1}{2}$in. PMT R960 from Hamamatsu Photonics, mounted with a fused silica window for UV measurements. The PMT current was read on an oscilloscope with GPIB interface. The apparatus was driven by computer under LabVIEW. A sketch of the experimental set-up is shown in Fig. 23. Measurements were acquired by programmable steps either in incident (Θ_I, Φ_I) or reflected (Θ_R, Φ_R) angle. The initialization procedure included a pedestal noise measurement via a shutter on/off control at the fiber entrance. The control of the mechanical precision was obtained by measuring the specular reflexion angle on a mirror located at the sample position. Overall calibrations of the detection scheme, including the lamp intensity spectrum and fiber wavelength transmission were performed at various stages of the light track from the source to the fiber head. This system allows to measure the semi-hemispherical Bidirectional Reflectance Diffuse Function (BRDF), defined as the ratio of the outgoing reflected radiance to the incoming irradiance [18]. In the comparative method we used here, BRDF was measured relative to a known reflectance material. We used as a reference the highly diffuse standard material Spectralon which is a hardened polytetrafluoroethyene (PTFE) manufactured by LabSphere Inc. and is a widely used white reference in the field of reflectometry. Its sphere integrated reflectivity is 99.5%. However, since the Spectralon sample was not easy to manipulate in our automatic set-up, our calibration procedure was realized in two steps. First we made an intermediate calibration at various angles and wavelengths, measuring reflectance of various highly diffusive materials such as PTFE foils, polyethylene fiber sheets (Tyvek) or ordinary white paper, relative to Spectralon. In the angular range of measurement, the closest reflectance to Spectralon was obtained for PTFE foils. While slightly less lambertian than Spectralon—the intensity of reflected light is greater in forward hemisphere—the PTFE foil was chosen in the calibration procedure: each experimental run was accompanied with a PTFE sample run to normalize and to avoid any variation in the experimental condition from one sample to another. Several ground samples were studied. Here we describe only the most significant ones relative to the ULTRA experiment at $\lambda = 360$ nm (the mean wavelength transmitted through the BG3 filter used in the experiment) and for an incident angle $\Theta_I = 25^\circ$ which corresponds to the most probable incident angle of showers detected by the ULTRA ground surface detector. Fig. 24 shows the raw measurement of outgoing radiance from the specular plane (i.e. $\varphi_R = 0^\circ$). A highly diffuse material like snow (a sample of which was collected in a cooled plate while it was snowing outdoor at a temperature of about $-3\,^\circ$C) was compared to the PTFE foil. Except for grazing angles greater than 70°, the reflectance of snow is almost 90% of PTFE. Water spectrum was obtained by filling a 10 cm depth cylindrical black vessel up to the reference sampling surface plane. Since this figure shows the reflectance on the incident plane, the specular reflexion peak is observed at 25°, wider than on a pure mirror reflecting surface even if here the log representation enhances the width appearance. The reflectivity drops

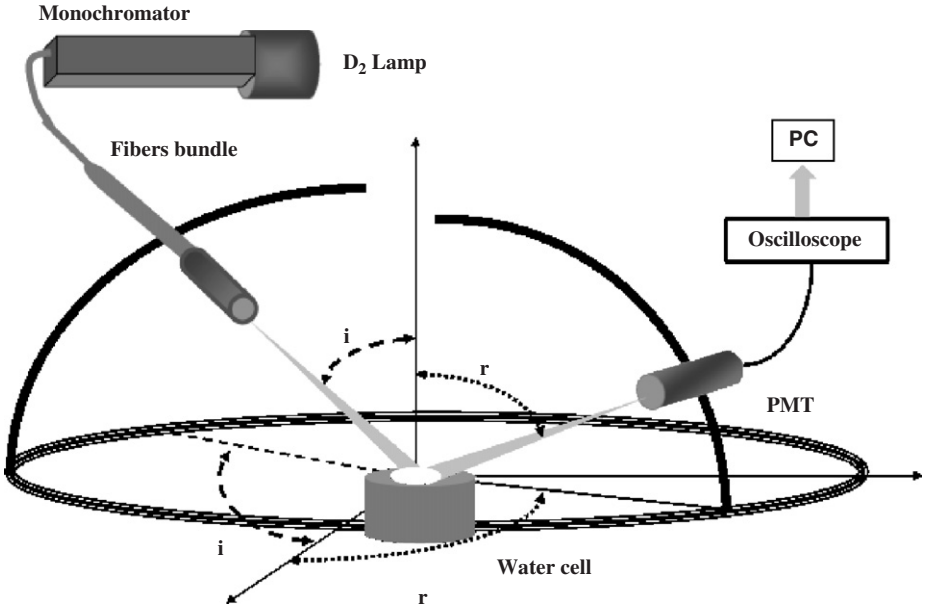

Fig. 23. Schematic view of the reflectometer set-up.

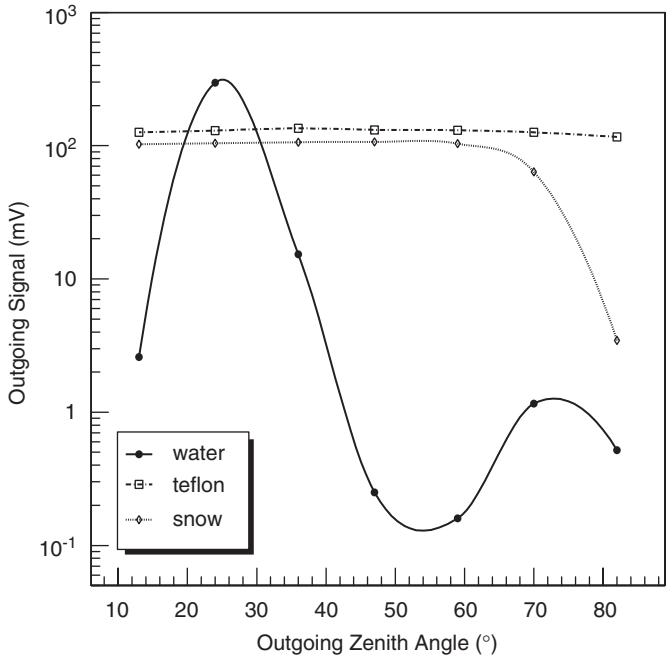

Fig. 24. Outgoing radiance at $\Theta_I = 25^\circ$ as a function of the outgoing zenith angle for various samples.

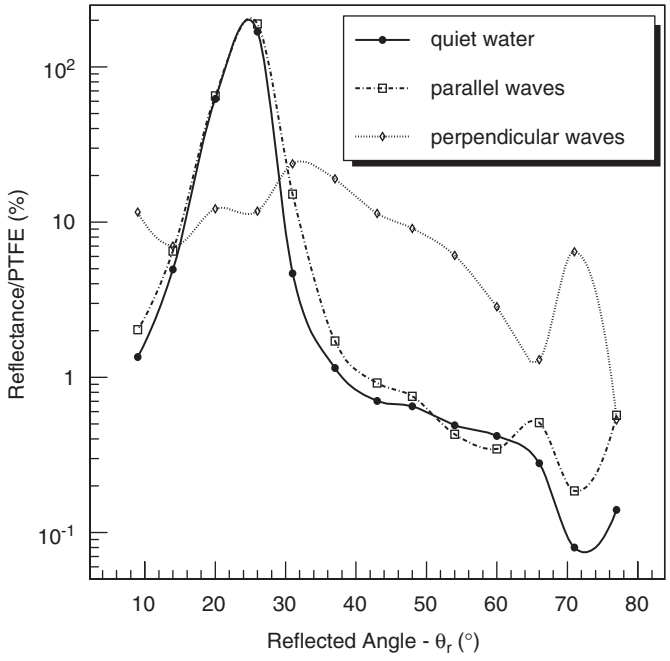

Fig. 25. Relative reflectivity at $\Theta_I = 25^\circ$ of quiet water (solid), water with parallel waves (dash-dotted) and water with perpendicular waves (dotted).

rapidly below 1% of PTFE away from the specular angle. A small bump, observed about 70°, is the contribution to the reflection due to the bottom of the vessel. The position and amplitude of this secondary peak vary with the depth of the vessel and the reflectivity of the bottom material.

In order to simulate the conditions of the ocean or Mediteranean Sea, where most of Cherenkov light signals are expected for EUSO or ULTRA measurements, we extended our measurement on water reflectivity by varying some sea surface parameters. We tried to simulate waves on the water surface by blowing compressed air through valve-regulated pipes directed at a grazing angle above the water surface. The intensity, stability and reproductibility of the generated waves were controlled via the waveform of the reflected light signal tuned on a long base time. The generated 'wind' speed never exceeded 0.2 m/s. While wavelengths and amplitudes, together with the vessel size, are rather far from oceanic conditions, this measurement somehow allowed us to predict the reflectivity of the sea. Fig. 25 shows the relative reflectivity on the specular plane of quiet water (a), water with parallel waves (b), and water with perpendicular waves. While in case (b) there is no strong change in the diffusion picture compared to (a), except for a slight widening of the specular peak and an increase at large angle, the case (c) of perpendicular waves behaves in a very different way: the specular peak almost disappears and the overall spectrum is more diffuse than in the two former cases. The angle at the impact of incoming light on a water wave is no longer at the fixed angle, refraction becomes more important, and volumic molecular diffusion becomes dominant. The vessel bottom effect is also observed in different conditions. On real sea one expects that the relative angle between shower Cherenkov light and wave direction will be a combination of both parallel and perpendicular angle depending on instantaneous local conditions. The result should show a variation of the order of a small percentage in sea reflectivity from shower to shower, specially at large zenith angles of reflection. This should be adjusted according to the real depth of the sea at the measurement location, and according to the sea water absorption factor depending upon the chlorophyll content.

7. Conclusions

The ETscope detector is a well characterized EAS array with good shower parameters reconstruction for $E \geqslant 3 \times 10^{15}$ eV, where the Cherenkov light signals are expected. The conversion from the acquired data to the photon density on the surface of the UV light detector lenses is well established and the energy threshold for both electromagnetic and Cherenkov detectors has been matched using the Monte Carlo simulation. Due to the very small expected diffuse signal, this energy threshold is very high, and we expect a very low rate of coincident events. Nevertheless, our main interest is to study the differences between the diffusion of photons with the spectral features of the Cherenkov emission and the true Cherenkov signal accompanied by the leptonic and hadronic components of the EAS. A few dozen events should be enough for this study. The data reduction and analysis of the events collected in Capo Granitola and the study of the diffused Cherenkov light from sea water will be presented and discussed in a future paper.

Acknowledgements

M. Dattoli would like to thank the National Institute for Astrophysics (INAF) for partly supporting her activity during this project.

References

[1] O. Catalano, P. Vallania, D. Lebrun, P. Stassi, M. Pimenta, M.C. Espirito Santo, ULTRA—Uv Light Transmission and Reflection in the Atmosphere. A supporting experiment for the EUSO Project, EUSO-SEA-REP-001-1 Technical Report, 4 January 2002.
[2] L. Scarsi, Il Nuovo Cimento 24-C (4–5) (2001) 471.
[3] O. Catalano, Il Nuovo Cimento 24-C (3) (2001) 445.
[4] EUSO-Extreme Universe Space Observatory, ⟨http://www.euso-mission.org⟩.
[5] A.E. Chudakov, in: Proceedings of the Symposium on Cosmic Rays, vol. 69, 1972, p. 69.
[6] R.A. Antonov, et al., Nucl. Phys. 52B (Proc. Suppl.) (1997) 182.
[7] C. Castagnoli, et al., Il Nuovo Cimento 6C (2) (1983) 202.
[8] I. Angelov, et al., in: Proceedings of the 27th ICRC, 2001, p. 900.
[9] S. Giarrusso, et al., Calibrazione di UVscope e BaBy e loro confronto: misure in laboratorio e misure di fondo UV notturno del cielo, Internal Report IASF-Pa/CNR 1/04, 2004.
[10] G. Agnetta, et al., in: Proceedings of the 29th ICRC, vol. 6, 2005, p. 169.
[11] O. Catalano, M.C. Maccarone, ULTRA Experiment—Report on the 'Capo Granitola' Campaign 2005, Internal Report IASF-Pa/INAF 2/05, December 13, 2005.
[12] Fresnel Technologies Inc., Forth Worth, Texas, USA, ⟨http://www.fresneltech.com⟩.
[13] P. Assis, P. Brogueira, L. Melo, M. Pimenta, J.C. Silva, J. Varela, in: Proceedings of the 28th ICRC, 2003, p. 947.
[14] M. Aglietta, et al., Nucl. Instr. and Meth. A 336 (1993) 310.
[15] D. Heck, J. Knapp, J.-N. Capdevielle, G. Schatz, T. Thouw, CORSIKA: a Monte Carlo code to simulate extensive air showers, Forschungszentrum Karlsruhe, Report FZKA 6019, 1998.
[16] S. Swordy, in: Proceedings of the 23rd ICRC, Rapporteur & Highlight papers, 1993, p. 243.
[17] G. Battistoni, C. Bloise, A. Ferrari, M. Monteno, V. Patera, E. Scapparone, Astroparticle Phys. 7 (1997) 101.
[18] Spectral reflectance, National Institute of Standard and Technologies, Special Publication 250-48.